Journal of Material Cycles and Waste Management (2023) 25:2087–2100
https://doi.org/10.1007/s10163-023-01655-2

ORIGINAL ARTICLE

Characterization and adsorption of raw pomegranate peel powder for lead (II) ions removal

A. Hashem[1] · Chukwunonso O. Aniagor[2] · M. Fikry[1] · Ghada M. Taha[1] · Sayed M. Badawy[3]

Received: 30 September 2022 / Accepted: 24 March 2023 / Published online: 25 April 2023

Abstract

The adsorption potential of raw pomegranate peel powder (PMPP) for lead (Pb) ions was investigated via batch mode at varying initial adsorbate concentration, contact time, and adsorbent concentration. The *PMPP* was extensively characterized using Fourier-transform infrared spectroscopy (FTIR), X-ray diffraction (XRD), Scanning electron microscopy (SEM), Energy-dispersion X-ray (EDX), thermogravimetry (TG), and differential scanning calorimetry (DSC) analyses. The instrumental characterization results confirmed the presence of important functional groups and surface texture/morphology that played key roles during the lead ion adsorption. Description of the experimental equilibrium data by nonlinear Langmuir, Freundlich, Dubinin–Radushkevich, and Temkin isotherm models was elaborately presented in the study. The experimental kinetic data were fitted to the Pseudo-first-order, Pseudo-second-order, Intra-particle diffusion, and Elovich models. The Temkin model satisfactorily predicted the isotherm data. Meanwhile, the intra-particle diffusion model was best at predicting the kinetic data at adsorbate concentration of 150 mg/L, while the Elovich model emerged as the best fit at 300 mg/L concentration. This study shows that lead ions could be efficiently removed using raw pomegranate peel powder.

Keywords Agro waste · Adsorption · Instrumental characterization · Pomegranate peel · Lead ion

Introduction

Lead (Pb) is a household element with extensive application in lead pigments, smelting, battery production, etc. [1]. Due to their remarkably high tensile strength, pliability, and low melting point, they serve as raw materials for the production of domestic utensils and as antiknock in automobiles [2, 3]. However, reports have shown that acute lead poisoning (in humans) inhibits the enzymatic, cellular, and organ functionality, thus leading to kidney failure, nervous system breakdown, etc. [4]. To forestall such negative health impact, a maximum permissible limit was set at 10 mg of Pb/liter of drinking water by the World Health Organization [5].

As a simple and cost-effective approach, adsorption techniques using a wide range of organic and inorganic adsorbents have been effectively applied in the sequestration of aqueous heavy metals in general and lead pollutants in particular. Recently, renewable and cheaply available agro wastes are considered viable alternatives to conventional organic and inorganic adsorbents [6, 7]. Ashfaq, et al. [8] investigated the lead ion sorption capacity of a biosorbent synthesized from a mixture of banana and potato peels. The maximum lead uptake was recorded at pH 5.0 using 1.0 g of adsorbent at 2 h contact time and 10 ppm initial adsorbate concentration. The effectiveness of distinct low-cost adsorbents synthesized from casuarina fruit, sorghum stem, and banana stem was also investigated for the uptake of lead ions [9]. The authors concluded that these adsorbents had promising potentials for adsorbing lead ions from industrial wastewater, thus contributing to environmental protection and sustainability. Furthermore, biosorbents prepared from corn and rice husks were studied for the removal of aqueous lead ions [10]. According to the authors, these biosorbents indicated more than 90% lead ion removal efficiencies.

In the present study, an efficient lead ion adsorbent was obtained from pomegranate peels by subjecting them to

✉ Sayed M. Badawy
sayedbadawy@hotmail.com

1 Textile Research Division, National Research Center, Dokki, Cairo, Egypt

2 Department of Chemical Engineering, Nnamdi Azikiwe University, P. M. B. 5025, Awka, Nigeria

3 National Center for Clinical and Environmental Toxicology, Faculty of Medicine, Cairo University, Cairo, Egypt

three physical processing stages namely, drying, crushing, and sieving. Pomegranate peels are mostly sourced as one of the byproducts of the pomegranate juice industry. According to available records, about 669 kg of these byproducts (piths, rinds, and peels) are generated from the processing of a ton of pomegranate fruit [11]. Notably, the peels and the internal membrane constitute about 50% of the entire pomegranate fruit [12]. Asides from their ready availability, pomegranate peels have several inherent functional groups that play key roles during pollutant adsorption and also permit the occurrence of multiple mechanisms. For instance, the hydroxybenzoic (gallic and ellagic) acids, derivatives of flavones, and hydroxycinnamic acids are responsible for their superior heavy metal chelation properties [13]. The phenolic compounds and the anthocyanin derivatives contribute to the excellent surface adsorption of free metal ions [14]. In a previous phytochemical investigation of pomegranate peels, 10 phenolic compounds containing a common hexahydroxy diphenol moiety were isolated [15]. In pomegranate peels, the main phenolic compounds reported in the literature include flavonoids, tannins, and phenolic acids [16].

The reported presence of elements (like sodium, Na; potassium, K; calcium, Ca; magnesium, Mg; nitrogen, N, etc.) and some complex polysaccharides could initiate the formation of important complexes during heavy metal adsorption [17]. Similarly, the electrically charged functional groups (such as the amino, hydroxyl, and carboxylic groups) on the peels provide strong binding sites for the aqueous heavy metal ions [18].

Within the last decade, several authors have investigated the heavy metal adsorption potentials of raw pomegranate peel powder (*PMPP*) [13, 14, 19–28]. The novelty of the current study lies in the authors' succinct discussion of the experimental results in comparison with findings from pertinent publications. Description of the experimental equilibrium data by nonlinear Langmuir, Freundlich, Dubinin–Radushkevich, and Temkin isotherm models was elaborately presented in the study. Non-linear regression analysis is preferable to determine isotherm and kinetic parameters. Previous investigations have shown that the nonlinear method is a better method than the linear method for fitting the kinetics of adsorption process [29, 30]. The nonlinear kinetic transformations to linear kinetic usually result in parameter estimation error and fit distortion. Furthermore, the *PMPP* was extensively characterized using Fourier-transform infrared (FT-IR) spectroscopy, X-ray Diffraction (XRD), Scanning electron microscopy (SEM), Energy diffraction X-ray (EDX), thermogravimetric analysis (TGA), and Differential scanning calorimetry (DSC) measurements. The effect of process variables was also investigated experimentally via a batch mode.

Materials and methods

Materials

Pomegranate peels were collected from fresh juice stores at a local market in Cairo, Egypt. The lead acetate (99%), sodium hydroxide pellets (97%), ethylene-diamine-tetra-acetic acid powder (98.5%), nitric acid (70%), sodium carbonate, acetone (99%), ethyl alcohol (95%), and all other reagents used in the study were laboratory-grade chemicals (Merck, Germany).

Preparation of pomegranate peel adsorbent

The collected pomegranate peels were cut into small pieces and washed with distilled water to remove inherent dust and dirt. The washed sample was soaked overnight in double distill water and afterward filtered off. This overnight soaking in water and filtration was repeated severally until all color and soluble materials were removed from the pomegranate peels. The decolored peels (*PMPP*) were oven-dried at 105 °C for 3 h, crushed to desired particle size (120 µm), and stored in an air-tight container for further use.

Batch adsorption studies

0.3 g of the *PMPP* was weighed into 125 mL Erlenmeyer flasks containing 100 mL of varying Pb(II) ion solution (100–600 mg/L). The pH of the initial solution was 7. The adsorption experiment was typically dynamic at 150 rpm, 30 °C, and a pre-defined period. After each adsorption experimental run (at a known initial adsorbate concentration), the spent *PMPP* was filtered off and the lead ion concentration in the supernatant was measured via the metal–ligand complexation titrations approach using a standard EDTA solution (0.0005 M). All experiments were repeated 3 times. The equilibrium adsorption capacity, q_e (mg/g) of the *PMPP* sample is evaluated from Eq. (1).

$$q_e = \frac{\left(C_o - C_e\right) * V}{W} \tag{1}$$

where C_o and C_e (mg/L) are the lead ion concentration at the onset of experiment and equilibrium, respectively, W (g) = mass of *PMPP* used, and V = volume of Pb(II) solution(0.1 L).

Instrumental characterization procedures

The pre- and post-adsorption FTIR spectra of the *PMPP* were determined using Perkin–Elmer

spectrophotometer from 4000 to 400 cm^{-1} using KBr disks containing ~ 5–10 mg of sample in ~ 300 mg of KBr. The XRD patterns were obtained on a PANalytical diffractometer (X'Pert PRO) in continuous scanning mode using a Cu tube (in the reading range of 2–80°). Solid samples are prepared for X-ray diffraction by grinding. The SEM micrograph of the *PMPP* was obtained (after overlaying the sample with a thin layer of gold using a diode sputter unit) on a scanning electron microscope (model JEOL-JSM-5600), at an accelerating voltage of 25.0 kV. Elemental analysis of the samples was obtained using an EDX spectrometer (Oxford Instruments 6587 EDX detector), attached to the JEOL-JSM-5600 unit used for SEM analysis. Thermogravimetric analysis (TGA) and differential scanning calorimetry (DSC) measurements were obtained using Themys thermal analyzer (SETARAM labsys TG-DSC-16). The samples were weighted to 13–15 mg in an aluminum crucible and introduced to the thermal analyzer with a measuring temperature range from room temperature up to700 °C with a heating rate of 10 °C/min under nitrogen atmosphere.

Results and discussion

Instrumental characterizations

Fourier-transform infrared (FTIR) spectroscopy

The FTIR spectra of the native and loaded *PMPP* are presented in Fig. 1. The native *PMPP* sample exhibited a broad absorption peak at 3291 cm^{-1}, indicating the presence of bonded and free hydroxyl groups, due to the O–H groups' vibrations (carboxylic acid, phenol, or alcohols) of cellulose, lignin, hemicellulose, and adsorbed water [31]. The peak observed at 2917 cm^{-1} corresponds to the C–H stretching vibration in the methyl groups, while those at 1711 cm^{-1} represent C = O stretching of the carbonyl group of aldehydes and ketones. The band at 1602 cm^{-1} is assigned to the CH_2 stretching of an aromatic ring from the hemicellulose. The strong stretching vibration of C–O at 1011 cm^{-1} is attributed to carboxylic acid, alcoholic, phenolic, ether, and ester groups of lignin and hemicelluloses components [19]. So far, the FTIR discussion has established the existence of five major absorption peaks on the native *PMPP* at 3291, 2917, 1711, 1602, and 1011 cm^{-1}. Similar absorption peaks were reported by others during the FTIR investigation of the raw pomegranate peel powder. For instance, Ben-Ali, et al. [19] observed these main peaks at 3298.68, 2941, 1713, 1607.21, and 1029.18 cm^{-1}, while Giri, et al.'s [13] findings coincided with 3402.05, 2926, 1735, 1619, and 1044 cm^{-1} peaks. Other weak peaks were recorded at 1320 and 1439 cm^{-1}. The peaks at 1320 cm^{-1} (δsCH_3) and 1439 cm^{-1} ($\delta asCH_3$, $\delta asCH_2$) are attributed to symmetric and asymmetric bending vibration of δCH_3 and δCH_2 scissoring in hemicelluloses (H_3C–(C = O)–O–) and lignin (H_3C–O–Ar), respectively [32]. The spectral line of loaded *PMPP* when compared to those of native *PMPP* shows a negligible change in the IR spectrum except the shrinking of the peak at 1711 cm^{-1} which corresponds to the carbonyl group stretching in aldehydes and ketones.

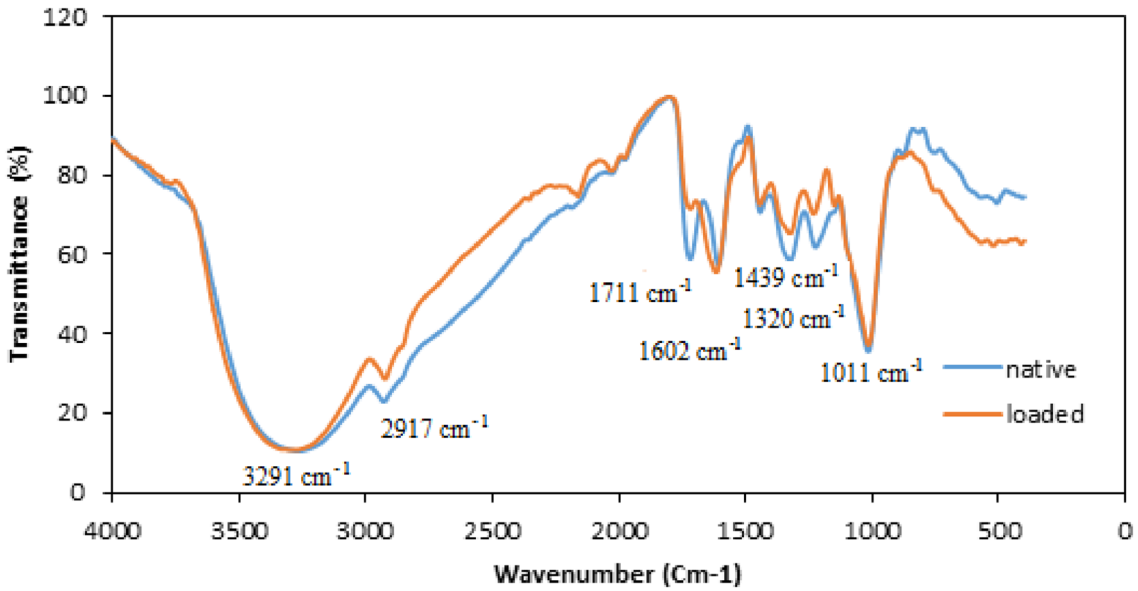

Fig. 1 FT-IR of Pomegranate Peel and Pb (II) loaded Pomegranate Peel

X-ray diffraction (XRD)

The X-ray diffraction pattern of the native *PMPP* (Fig. 2a) shows weak peaks at 17.14°, 22.11°, and 44.5°. Incidentally, these peaks were superimposed onto an amorphous diffraction spectrum, thus indicating the presence of a sublime crystalline cellulose I_β structure [33]. The absence of the sharp diffraction peaks of the crystalline cellulose and the predominance of amorphous peaks in the XRD spectrum indicates that the non-cellulosic (hemicellulose and lignin) components are the main contents of the native *PMPP*. Figure 2b shows no observable change in the amorphous phase of the native *PMPP* after complexation with the aqueous lead ions. Hence, it is believed that the complexation of leads ions with the *PMPP* functional groups occurred at the same component phases. The present study on the application of raw pomegranate peel powder in heavy metal adsorption did not investigate the surface crystallinity of their respective adsorbent samples.

Scanning electron microscopy (SEM)

Figures 3 (a and b) shows the morphology of the surface of native and loaded *PMPP*. The SEM micrograph shows a soft amorphous and heterogeneous structure of typical non-cellulosic contents (lignin and hemicellulose). Also, the absence of orientation and fibrous structure of cellulose and porosity was observed. This finding coincides with the XRD and FTIR analyses result, thus confirming that the main components of the *PMPP* sample are non-cellulosic materials. Studies by Salam, et al. [14] and Giri, et al. [13] reported a coarse surface structure with hollow cavities and pore structure on the native/raw pomegranate peel. However, the coarse and rough surface structures metamorphized into a comparatively smoothened surface due to a possible occurrence of a redox reaction between the adsorbent active sites and adsorbed chromium ions. Conversely, Ghaneian, et al. [20] made a differing observation, as they reported a significant morphological modification in the pomegranate peel powder adsorbent from smooth (before adsorption) to rough morphology (after heavy metal biosorption).

The EDX spectrum demonstrated that the major elements of native *PMPP* were carbon (47.71%), oxygen (50.25%),

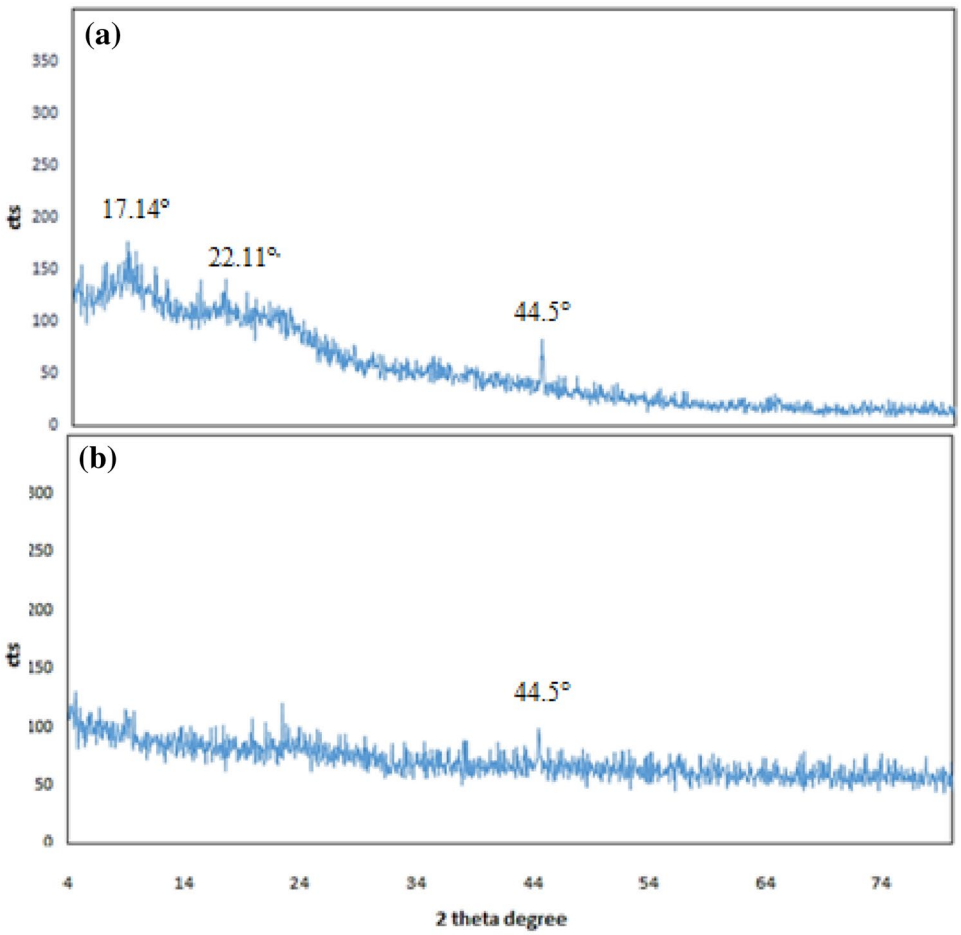

Fig. 2 XRD of Pomegranate Peel and Pb (II) loaded Pomegranate Peel

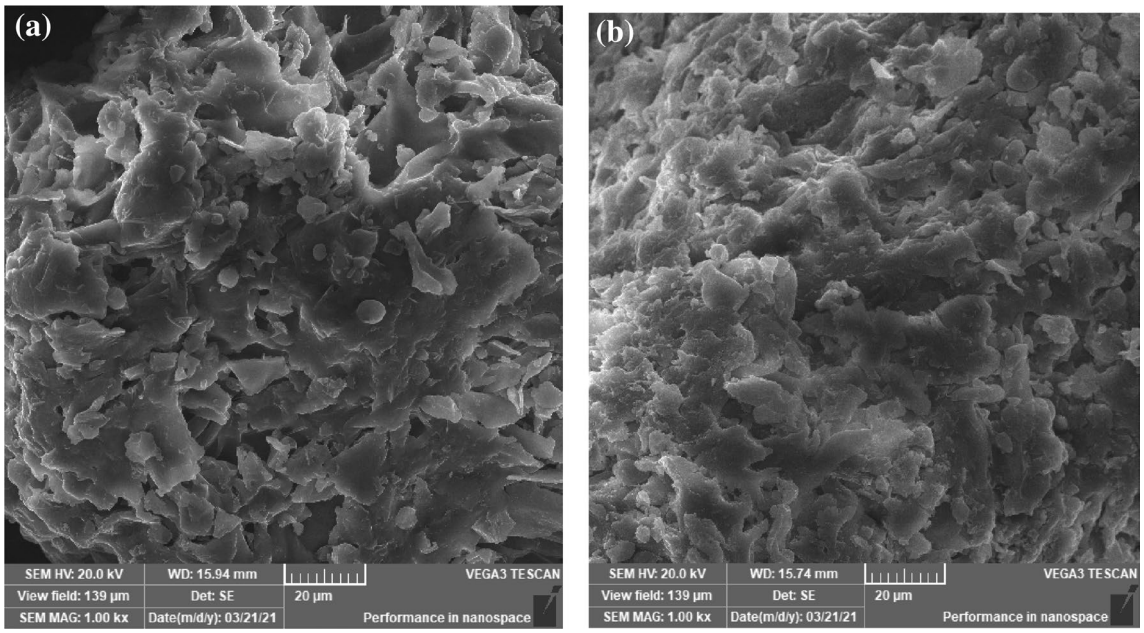

Fig. 3 **a** SEM of Pomegranate Peel. **b** SEM of Pb (II) loaded Pomegranate Peel

and nitrogen (1.66%) [Fig. 4 (a and b)]. The presence of Pb (0.38%) on the surface of *PMPP*, clearly demonstrates that lead ions were successfully adsorbed. Other authors also reported the presence of carbon, oxygen, nitrogen, and hydrogen as the major constituents of PMPP [13, 19]. However, asides from the main constituents, traces of potassium, calcium, copper, zinc, manganese, iron were also observed by [13, 14].

Thermal analysis

The thermal behavior of the native *PMPP* was studied using thermogravimetry (TG), differential thermogravimetry (DTG), and differential scanning calorimetry (DSC) analyses under nitrogen atmosphere and heating rate of 10 °C min^{-1}. Figure 5a shows TG and DTG curves for the native *PMPP*. The thermal weight loss of the sample proceeds in multi-steps with a total mass loss of 63wt% in a temperature range of 133–500 °C. The first step with a weight loss of 8% at 58–133 °C is attributed to the evolution of moisture. The multi-decomposition at 194–334 °C is attributed to the degradation of the hemicellulose, lignin, and cellulose [19, 34]. Furthermore, the multi-decomposition of the raw *PMPP* is associated in the DSC thermogram with an exothermic peak (91.96 j/g) at the initial main decomposition with a temperature range 136–218 °C and an endothermic peak (−40. 48 j/g) at the end of the main decomposition peak with a temperature range 309–368 °C (Fig. 5b). The lignin has a wider degradation temperature range than cellulose and hemicellulose with a maximum weight loss at 240 and 334 °C due to its constituent functional groups, such as phenolic, hydroxyl, carboxyl, carbonyl, and methoxy groups [34]. The thermogravimetric data indicate that the native *PMPP* is thermally stable up to 143 °C.

Effect of process variables

The effect of pH on adsorption capacity (mg/g) of Pb(II) onto pomegranate peel is shown in Fig. 6. With the increase in pH of solution pH (from pH 2.0 to 5.5), the amount of lead adsorbed significantly increased (from 0 to 335 mg/g). Adsorption decrease was observed at a pH greater than 6.0 as a result of Pb (II) ion precipitation as $Pb(OH)_2$. The effect of adsorbent concentration on the lead uptake capacity as illustrated in Fig. 7(a) shows the highest lead uptake (335 mg/g) at 0.3 g/L adsorbent concentration and reaction conditions: Pb(II) ion con., 300 mg/L; pH, 5.5 and temp., 30 °C. The uptake values decreased progressively with a further increase in adsorbent concentration. It is well known that such improved heavy metal uptake at lower adsorbent concentration is related to the availability of more sorption sites [35]. Other authors who investigated the heavy metal sorption ability of raw pomegranate peel powder reported a similar improvement in the cation uptake (q_e) at lower adsorbent concentration due to greater sorption site availability. Hence, 0.3 g/L was adopted as the optimum adsorbent concentration in the study.

The combined effect of contact time and adsorbate concentration as presented in Fig. 7(b) shows a consistent increase in the amount of lead ion adsorbed as the

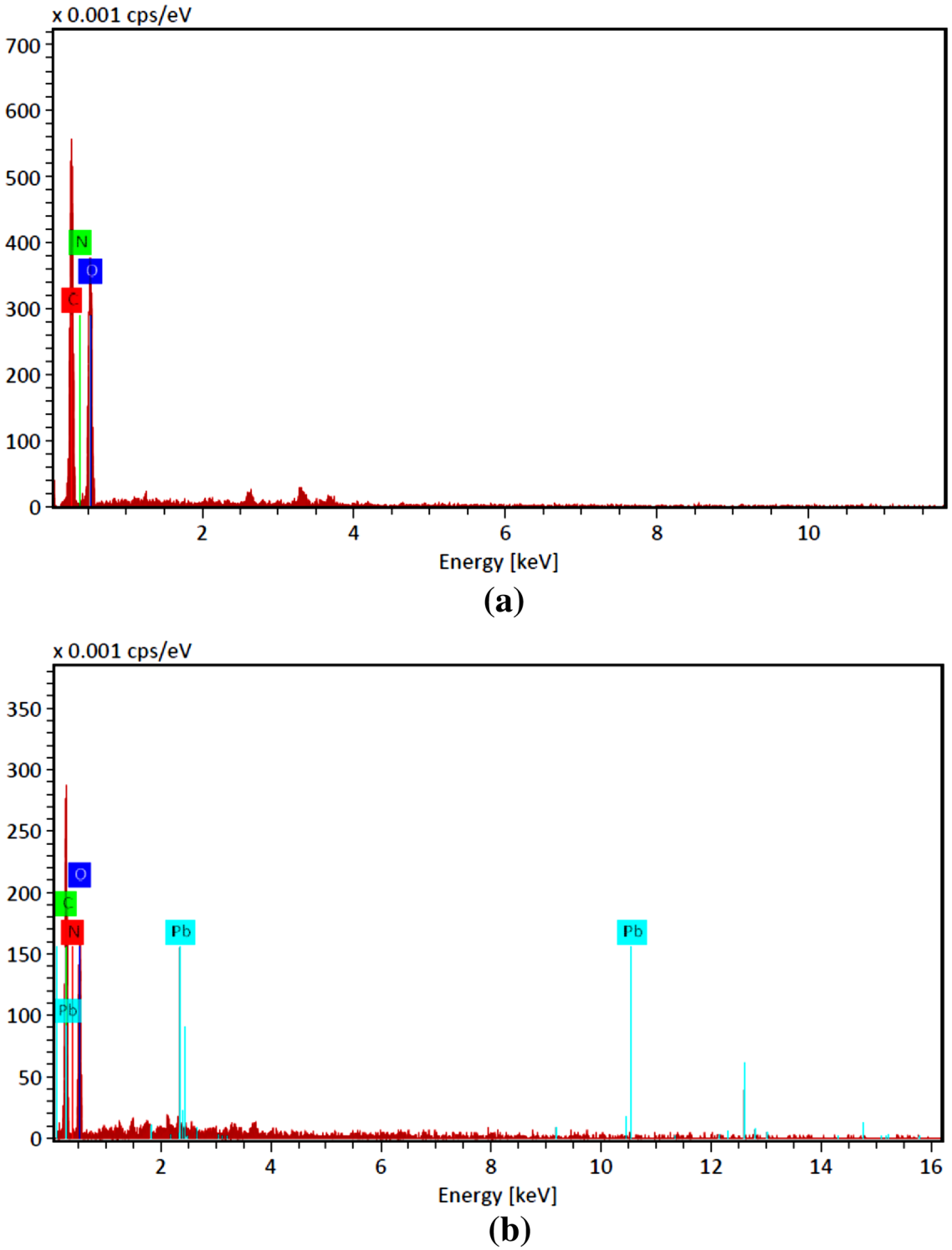

Fig. 4 **a** EDX of Pomegranate Peel. **b** EDX of Pb (II) loaded Pomegranate Peel

adsorption time extends. Notably, the q_e (mg/g) value appreciated significantly within the first 60 min at 150 mg/L and 300 mg/L Pb(II) ion concentration.

The observed variation in the q_e (mg/g) value at varying initial concentrations is attributed to changes in concentration gradient within the bulk adsorbate phase [36]. At 300 mg/L adsorbate concentration, increased sorption

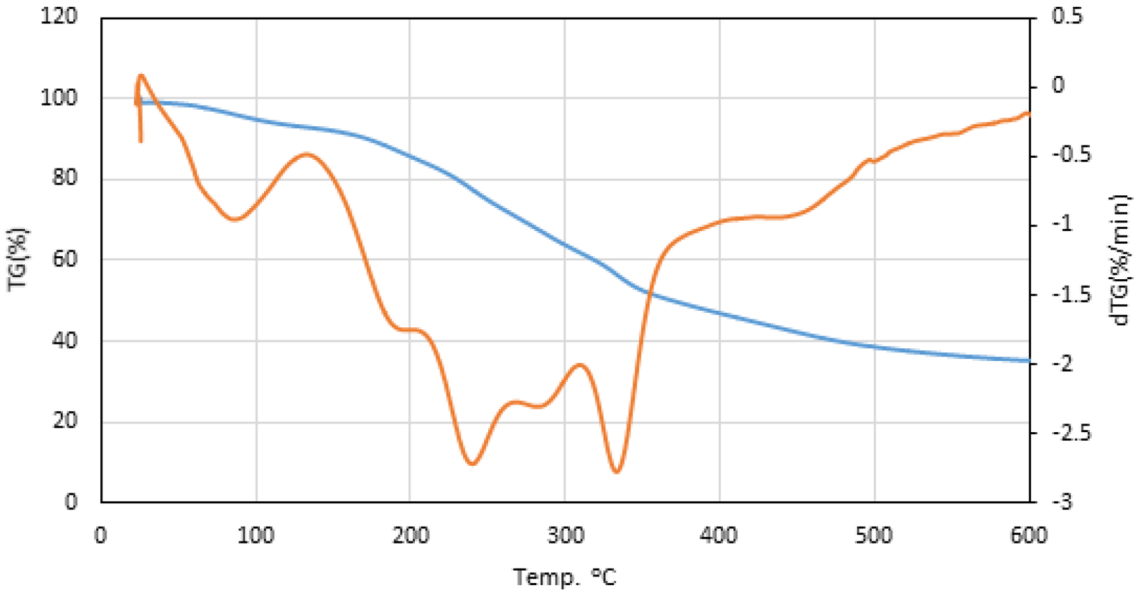

(a) TGA of raw Pomegranate Peel

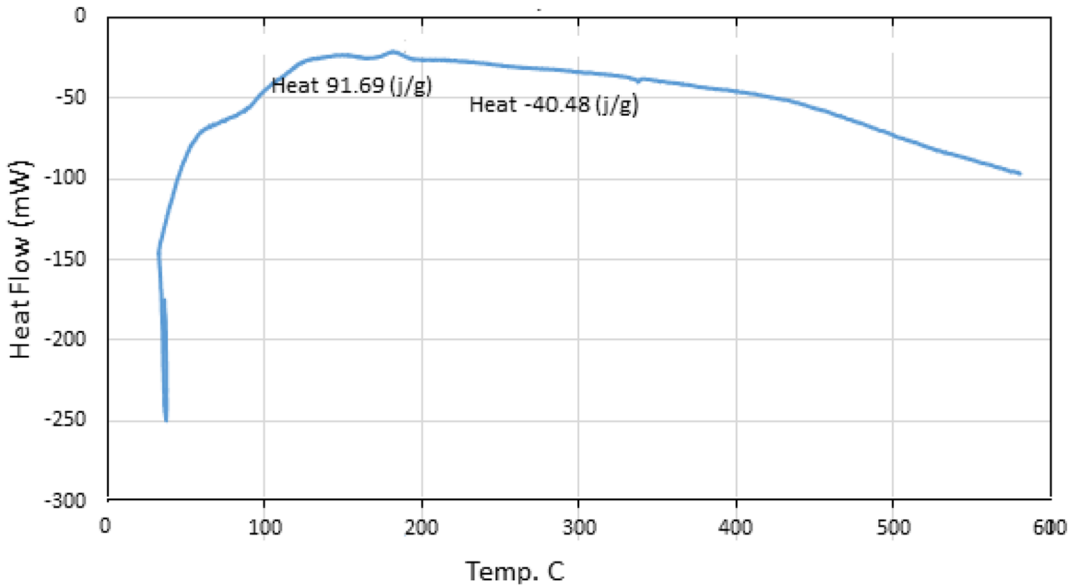

(b) DSC of raw Pomegranate Peel.

Fig. 5 TGA and DSC of Pomegranate Peel

driving force predominates due to the existence of a larger concentration gradient. This development ensures the complete saturation of the available *PMPP* active sites by the lead ions, thus resulting in higher adsorptive uptake per gram of adsorbent [37]. Similarly, the progressive increase in the q_e (mg/g) value with the rise in contact time is attributed to improvement in surface area and porosity, as well as minimal pore diffusion resistance within the *PMPP* matrix sequel to their swelling in the adsorbate solution.

Adsorption isotherm modeling

Adsorption isotherms provide insight into the nature of adsorbate–adsorbent interaction within an adsorption system at equilibrium (dynamic balance in adsorbate and adsorbent

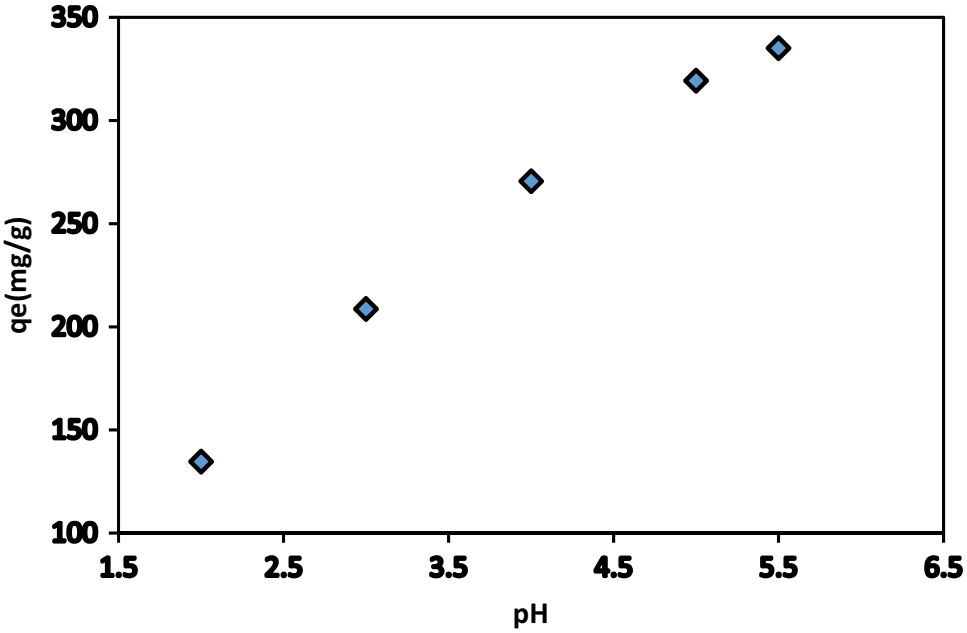

Fig. 6 Effect of pH on adsorption capacity of Pb(II) onto Pomegranate Peel; Reaction conditions: Pb(II) ion conc., 300 mg/l; Adsorbent conc., 0.3 g/l; temp., 30 °C; contact time, 2 h

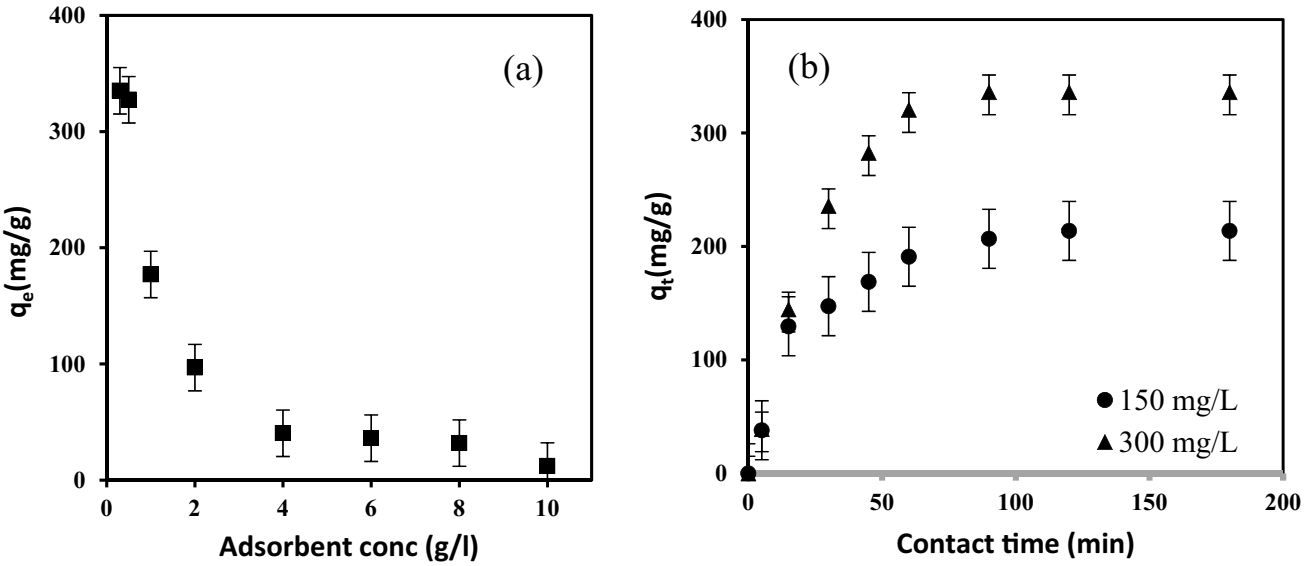

Fig. 7 The graphical representation of the effect of **a** adsorbent concentration, Pb(II) ion con., 300 mg/L, **b** contact time and initial adsorbate concentration on the adsorption capacity; Reaction conditions: Pb(II) ion con., 150 mg/L and 300 mg/L; Adsorbent conc., 0.3 g/L; pH, 5.5; temp., 30 °C

concentration). The nature of these interactions is often informed from the associated isotherm model constants [38]. In this study, the experimental equilibrium data were fitted to four widely used isotherm models namely, Langmuir, Freundlich, Dubinin–Radushkevich, and Temkin as shown in Fig. 8. The equations of the adsorption isotherm models are presented Table 1. The error distribution between the data of the predicted isotherm models and the experimental data was minimized using error functions to determine the most accurate model of the obtained isothermal data. The variance between predicted isotherm data and experimental data was optimized using the solver add-in of Microsoft Excel. The common error functions used for optimization of the isotherm parameters are (Table 2): average percentage error (APE%), average relative error (ARE), a determinant of the quality of the fit (χ^2), hybrid fractional error function (HYBRID), and normalized standard deviation (Δq%).

The best adsorption isotherm was predicted by normalizing the error functions and finding the sum of normalized error (SNE). This procedure involves the division of

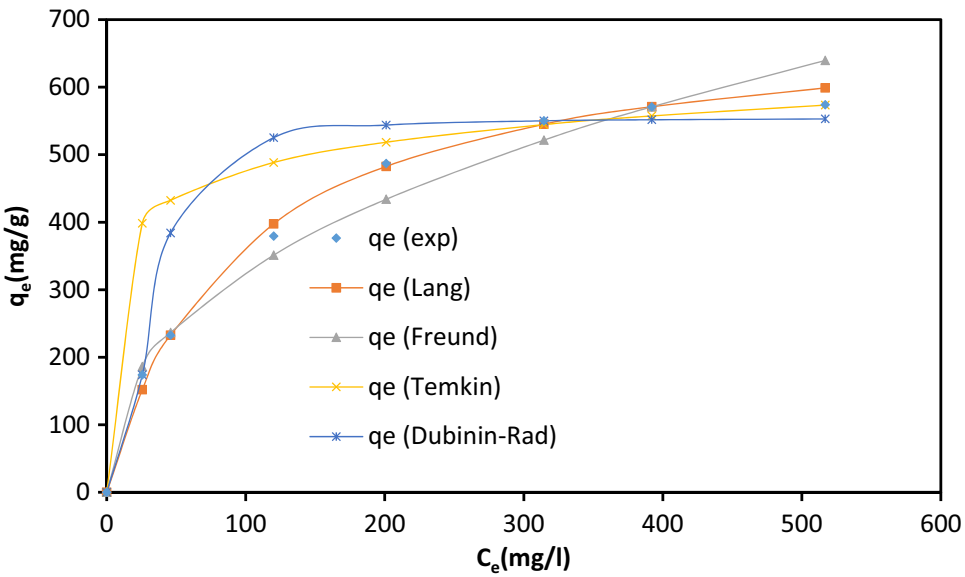

Fig. 8 Comparison between two-parameter isotherm models and experimental data (exp) obtained for adsorption on Pb(II) ions onto Pomegranate Peel at 30 °C; Reaction conditions: pH,5.5; adsorbent conc., 0.3 g/L; temp., 30 °C; time, 2 h

Table 1 Equations of two-parameter isotherm and adsorption kinetic models

Two-parameter isotherm models	Parameters	Adsorption kinetic equations	Parameters
Langmuir $q_e = \frac{k_L.C_e}{1+a_L.C_e}$	a_L	Pseudo-first order $q_t = q_e\left[1 - exp\left(-k_1 t\right)\right]$	k_1
	K_L		q_e
Freundlich $q_e = K_F.C_e^{1/n}$	1/n	Pseudo-second order $q_t = \frac{k_2 q_e^2 t}{(1+k_2 q_e t)}$	K_2
	K_F		q_e
Temkin $q_e = \frac{RT}{b_T} \bullet ln\left(A_T C_e\right)$	A_T	Intra-Particle Diffusion $q_t = k_{id} t^{0.5} + q_e$	K_{id}
	b_T		q_e
Dubinin–Radushkevich $q_e = q_D.\exp(-B_D[RT\ln(1+\frac{1}{C_e})]^2)$	q_D	Bangham's Equation $q_t = q_e\left[1 - exp\left(-k_b t^n\right)\right]$	q_e
			n
	B_D		k_b
		Elovich Equatio $q_t = \beta ln(\alpha\beta t)$	α
			B

all the error values obtained for the different error function models with the lowest error value and their subsequent summation to generate the minimum normalization error, SNE. Judging from the magnitude of the sum of normalized error values (SNE), all the studied models provided a good description of the experimental equilibrium data (Table 3). Detailed interpretation of the data fittings of the respective isotherm model in comparison with published literature is presented in subsequent subheadings.

Langmuir model

From the model-generated constants presented in Table 3, the Langmuir model depicted a reasonably low sum of normalized error (SNE) value, thus indicating a good model fit. A maximum adsorption capacity (q_{max}, mg/g) value of 600 mg/g was obtained at ambient temperature. This value is quite high and depicts a strong affinity between the lead ions and the PMPP due to the strong metal–ligand interaction with Pb(II) ion in aqueous solutions compared with divalent cations in addition to the presence of functional groups on the peels and small size of lead ion, which could favor for the accessibility of Pb(II) intercalation and diffusion more easily to the PMPP surface. Literature survey on the heavy metal adsorption application of raw pomegranate peel powder shows a relatively lower adsorption capacity (Table 4). Similarly, the K_L(L/mg) constant which is related to the energy of adsorption was found to be 7.55 in this study. This value is synonymous with high associated adsorption energy (a likely chemisorption process). Comparatively, the

Table 2 The applied goodness-of-fit models

Error Function	Equation
Average relative error (ARE)	$ARE = \sum_{i=1}^{n} \left\| \frac{(q_e)_{exp.} - (q_e)_{calc.}}{(q_e)_{exp.}} \right\|$
Average percentage error (APE)	$APE\% = \frac{\sum_{i=1}^{N} \left\| [((q_e)_{exp.} - (q_e)_{calc.})/q_{exp.}] \right\|}{N} x100$
Sum squares error (ERRSQ/SSE)	$ERRSQ = \sum_{i=1}^{n} [(q_e)_{calc.} - (q_e)_{exp.}]^2$
Hybrid fraction error function (Hybrid)	$Hybrid = \frac{100}{n-p} \sum_{i=1}^{n} [\frac{((q_e)_{exp.} - (q_e)calc.)^2}{(q_e)_{exp.}}]_i$
Marquardt's percent standard deviation (MPSD)	$MPSD = (\sqrt[100]{\frac{1}{n-p} \sum_{i=1}^{n} [\frac{((q_e)_{exp.} - (q_e)_{calc.})}{(q_e)_{exp.}}]^2}$
Nonlinear chi-square test (χ^2)	$\chi^2 = \sum \frac{(q_{e.exp} - q_{e.theoretical})^2}{q_{e.theoretical}}$
Coefficient of determination (R^2)	$R^2 = \frac{\sum_{i=1}^{n} (q_{e,calc} - \overline{q_{e,exp}})^2}{\sum_{i=1}^{n} (q_{e,calc} - \overline{q_{e,exp}})^2 + \sum_{i=1}^{n} (q_{e,calc} - q_{e,exp})^2}$

Table 3 Isotherm model parameters

Langmuir	Freundlich	Temkin	D–R
q_{max} = 707.424	$1/n_F$ = 0.41	K_T = 73.95	q_D = 554.53
K_L = 7.55	K_F = 49.16	b_T = 43.24	β_D = 1.2E-04
R_L = 0.011	R^2 = 0.994	R^2 = 0.940	R^2 = 0.895
R^2 = 0.999	**SNE = 1.026**	**SNE = 1.013**	E = 64.55
SNE = 1.059			**SNE = 1.014**

Bold indicates Sum of Normalized Error [SNE] value

Table 4 Maximum adsorption capacity reported in pertinent studies using raw Pomegranate peel powder

Maximum adsorption capacity (mg/g)	Adsorbate	Refs
165.9	Cr(VI)	[12]
30.12	Cu(II)	[17]
3.31	Cr(VI)	[18]
20.87	Cr(VI)	[11]
9.45	Cr(VI)	[19]
23.05	Cd(II)	[20]
193.9	Pb(II)	[21]
7.54	Ni(II)	[22]
8.98	Co(II)	[22]
166.63	Pb(II)	[23]
47.17	Cr(VI)	[24]
18.5	Fe(II)	[25]
6.18	NH_4(I)	[26]
600	Pb(II)	Present work

K_L values reported in the aforementioned pertinent literature were less than unity, except for the K_L = 2.76 reported by Giri, et al. [13]. The dimensionless separation factor, R_L, which is used to evaluate the feasibility and applicability of the process was found to be less than unity in the current study, as well as in the result presented by Salam, et al. [14] and Ben-Ali, et al. [19]. This finding is an indication of a favorable adsorption (since $0 < R_L < 1$).

Freundlich model

The Freundlich model depicted a good description of the experimental data judging from the low SNE value shown in Table 3. Also, the models' dimensionless constant "*n*" quantifies the adsorbent–adsorbate bond energy. If $0 < 1/n_F < 1$, then a favorable adsorption process is postulated. Table 3 shows $1/n_F$-value that is less than unity. This result is in line with the $1/n_F$ value of 0.30 [14], 0.40 [19], and 0.80 [21] reported during the adsorption removal of heavy metal using raw pomegranate peel powder. Similarly, the K_F value, which quantifies the bond strength, was relatively high (K_F = 49.16) and is in line with the value of 74.68 reported by Salam, et al. [14] during aqueous Cr(VI) adsorption onto pomegranate peel powder. Using similar adsorbents for heavy metal adsorption, Ben-Ali, et al. [19], and Mohammed, et al. [21] reported minimal bond strengths as expressed in much lower K_F-values of 3.98 and 3.15, respectively.

Temkin model

From the model-generated constants presented in Table 3, the Temkin model satisfactorily predicted the isotherm data. The nature of the adsorption process in terms of heat energy distribution is captured in the sign convention of the model's

b_T value. A positive value indicates an exothermic process, while a negative one is typical of an endothermic adsorption operation. From Table 2, a positive b_T value was recorded in the study. Hence, the lead ions were adsorbed onto the *PMPP* sites, with the liberation of some latent adsorption energy (exothermic process). Thus, lead binding onto *PMPP* is a low-temperature operation. Salam, et al. [14] and Ben-Ali, et al. [19] reported lower but positive b_T-values of 56.88 and 5.624 J mol^{-1} during the adsorption of Cr(VI) and Cu(II), respectively onto raw pomegranate peels powder.

Dubinin–Radushkevich (DR) model

This model is an important one due to its temperature dependence and the mean free energy, E (kJ/mol) term of the model. According to Aniagor, et al. [39], E (kJ/mol) defines the change in adsorption energy occurring when a mole of adsorbate migrates from the bulk fluid phase and attaches to the adsorbent surface. Consequently, the physical (physisorption) and the chemical (chemisorption) nature of an adsorption process is distinguished when $E < 8$ kJ/mol and $E > 8$ kJ/mol, respectively [40]. The E (kJ/mol) value obtained in this study (Table 2) suggests the existence of chemisorption. This conclusion was made earlier as informed from the Langmuir isotherm model analysis. Using similar raw pomegranate peel powder for Cr(VI) adsorption, Salam, et al. [14] reported an E (kJ/mol) value of less than 8.0 kJ/mol, thus a probable physi-sorption process. The study also noted an increase in the E (kJ/mol) values from 1.17 to 4.46 kJ/mol as the operating temperature appreciated from 303 to 323 K. Similarly, Ben-Ali, et al. [19] obtained E (kJ/mol) values in the range of 32.596 kJ/mol to 40.572 kJ/mol during the adsorption of Cu(II) onto raw pomegranate peel powder. Thus, a chemisorption interaction between the adsorbate and adsorbent was postulated.

Adsorption kinetics modeling

For the kinetics studies, four nonlinear models were utilized as shown in Fig. 9. The nonlinear equations of the adsorption kinetics models are presented in Table 1. Judging from the low SNE values depicted in Table 5, all the studied models provided a good description of the experimental kinetics data. The intra-particle diffusion model was best at predicting the kinetic data at adsorbate concentration of 150 mg/L, while the Elovich model emerged as the best fit at 300 mg/L concentration.

The Pseudo-first-order (PFO) model-generated constants, as presented in Table 5, shows a slight variation in the first-order rate constant (k_1) with an increase in the initial adsorbate concentration. The same could not be said about the calculated adsorption capacity (q_{ecal}), as the value significantly increased as the initial concentration. A similar observation was made by Ben-Ali, et al. [19] and Ghaneian, et al. [20] during the application of raw pomegranate peel powder in heavy metal sorption, as they reported a slight and inconsistent variation in the k_1 values with the increase in initial adsorbate concentration. The authors did not explain the observed data inconsistency. Similarly, the increment in the $q_{e\,cal}$ value (from the aforementioned studies) as a function of initial concentration increase was also irregular. Giri, et al. [13] reported a negative k_1-value which is indicative of the poor fitting of the Pseudo-first-order model to the experimental kinetic data.

The Pseudo-second-order rate constant (PSO), k_2 at 150 mg/L initial adsorbate concentration was found to be higher than the one recorded at 300 mg/L initial adsorbate

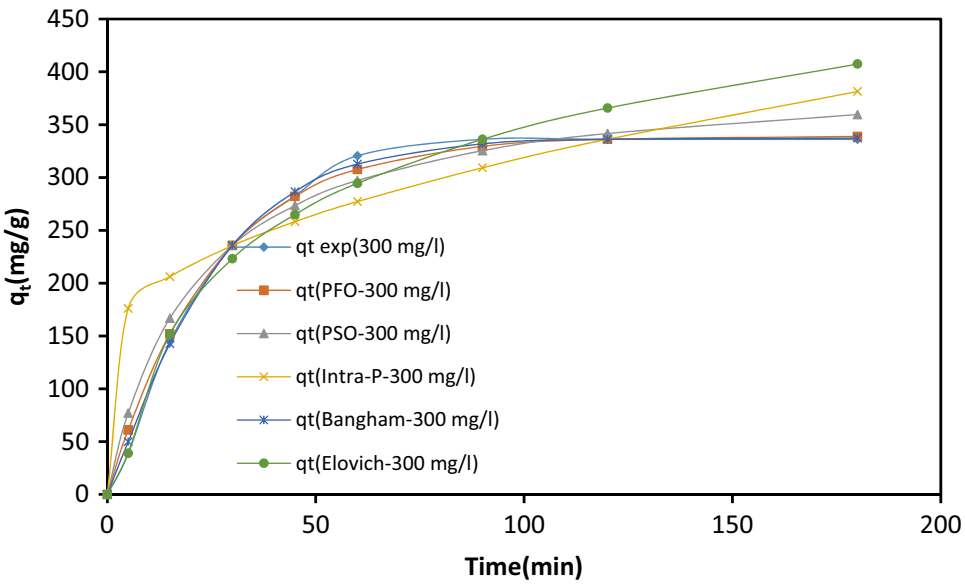

Fig. 9 Comparison between kinetic models and experimental data (exp) obtained for adsorption on Pb(II) ions onto Pomegranate Peel; Reaction conditions: Pb(II) ion con., 300 mg/L; Adsorbent conc., 0.3 g/L; pH, 5.5; temp., 30 °C

Table 5 Kinetic model parameters

Pseudo-first-order	Pseudo-second-order	Elovich	Intra-particle diffusion
C_o = 150 mg/L			
q_e = 94.50	q_e = 104.66	α = 32.696	K_{id} = 11.870
k_1 = 0.039	k_2 = 2.0E-04	β = 0.020	c = 83.658
R^2 = 0.995	R^2 = 0.996	R^2 = 0.995	R^2 = 0.974
SNE = 1.058	**SNE = 1.095**	**SNE = 1.090**	**SNE = 1.056**
C_o = 300 mg/L			
q_e = 151.86	q_e = 166.77	α = 30.048	K_{id} = 18.371
k_1 = 0.040	k_2 = 1.18E-04	β = 9.7E-03	c = 134.883
R^2 = 0.998	R^2 = 0.995	R^2 = 0.990	R^2 = 0.956
SNE = 1.111	**SNE = 1.068**	**SNE = 1.029**	**SNE = 1.038**

Bold indicates Sum of Normalized Error [SNE] value

$q_{e.exp}$ @ 150 mg/L = 129.60 mg/g

$q_{e.exp}$ @ 300 mg/L = 144.65

concentration. Hence, the k_2-value decreased with increasing adsorbate concentration. This could be due to the presence of adsorbent sites that is large enough to absorb all the available adsorbate molecules within the 150 mg/L adsorbate concentration system. With an increase in the initial adsorbate concentration, the adsorption rate constant value dropped slightly due to limited adsorption sites (since there was no corresponding increase in the adsorbent concentration). Studies by Ghaneian, et al. [20], and Salam, et al. [14] reported a consistent decrease in the k_2 values with an increase in the initial adsorbate concentration, while Ben-Ali, et al. [19] observed inconsistency in the k_2 values. The $q_{e\ cal}$ value obtained in this study was further found to consistently increase as the initial adsorbate concentration. This finding is in line with the variation in $q_{e\ cal}$ values reported by Ghaneian, et al. [20].

In the case of the Elovich model, minimal numerical differences were observed between the initial adsorption rate (α) and desorption constant (β) values at varying initial adsorbate concentrations. Incidentally, both constants decreased with increasing initial adsorbate concentration. The aforementioned explanation regarding adsorbent site depletion at higher adsorbate concentration (paragraph 2 of this section) still explains the decrease in the α value, with concentration increase from 150 mg/L to 300 mg/L. Also, the desorption rate expressed as the β values reduced due to initial concentration increase, as reflected in the improved adsorption capacity recorded at higher concentration in the case of Pseudo-first-order (PFO)and Pseudo-second-order (PSO) models. The Elovich model constants obtained by Ghaneian, et al. [20] followed the same trend as those reported in this study. The α- and β-values reported by other authors [19] varied inconsistently as the initial adsorbate concentration.

Regarding the intra-particle diffusion model, Table 5 shows an increase in the viscous drag occurring within the system with an increase in the initial adsorbate concentration. This is expressed in the magnitude of the boundary layer thickness (*c* values). Accordingly, the lower the *c* value, the weaker the viscous drag and vice versa. Hence, the c-value which increased from 83.66 (at 150 mg/L initial adsorbate concentration) to 134.88 (at 300 mg/L initial adsorbate concentration) implies an increase in the viscous drag. Despite the perceived drag, the intra-particle diffusion-controlled sorption rate (k_{id}) was still more at 300 mg/L adsorbate concentration and also explains the higher adsorption capacity recorded in the case of Pseudo-first-order (PFO) and Pseudo-second-order (PSO) models at higher initial adsorbate concentrations.

Conclusion

Based on the conducted literature survey, only a few authors reported the lead adsorptive application of raw pomegranate peel powder (*PMPP*). Hence, this present research investigated the adsorptive potentials of raw pomegranate peel powder for the adsorption of aqueous lead pollutants. Experimental findings show the dependence of *PMPP* adsorption capacity on adsorbent concentration, contact time, and initial lead ion concentration. The adsorption process was studied over an extended 3 h period. However, the maximum lead ion uptake was attained within the first 60 min. Pomegranate peel powder showed a high affinity to adsorb lead ions. The experimental equilibrium data correlated well with the nonlinear forms of Langmuir, Freundlich, Temkin, and Dubinin–Radushkevich isotherms models. The Temkin model satisfactorily predicted the isotherm data. Similarly, effective kinetics data modeling and description were achieved using the Pseudo-first-order, Pseudo-second-order, Intra-particle diffusion, and Elovich models. The intra-particle diffusion model was best at predicting the kinetic data

at adsorbate concentration of 150 mg/L, while the Elovich model emerged as the best fit at 300 mg/L concentration.

Author contributions AH: Conceptualization, Methodology, Writing—original draft. COA: Interpretation, discussion. MF: Visualization. GMT: Methodology, Data curation. Funding. S.M. Badawy: Methodology, Writing—original draft.

Funding Open access funding provided by The Science, Technology & Innovation Funding Authority (STDF) in cooperation with The Egyptian Knowledge Bank (EKB). "Not applicable".

Data availability "Not applicable".

Declarations

Conflict of interests The authors declare that they have no known competing financial interests or personal relationships that could have appeared to influence the work reported in this paper.

Ethical approval "Not applicable".

References

1. Hashem A, Aniagor C, Taha GM, Fikry M (2021) Utilization of low-cost sugarcane waste for the adsorption of aqueous Pb (II): kinetics and isotherm studies. Curr Res Green Sustain Chem 4:100056
2. Hashem A, Ahmad F, Fahad R (2008) Application of some starch hydrogels for the removal of mercury(II) ions from aqueous solutions. Adsorpt Sci Technol 26(8):563–579
3. Sone H, Fugetsu B, Tanaka S (2009) Selective elimination of lead (II) ions by alginate/polyurethane composite foams. J Hazard Mater 162(1):423–429
4. Paz S, Rubio C, Frías I, Gutiérrez ÁJ, González-Weller D, Martín V, Revert C, Hardisson A (2019) Toxic metals (Al, Cd, Pb and Hg) in the most consumed edible seaweeds in Europe. Chemosphere 218:879–884
5. Caroli S, Forte M, Nuccetelli C, Rusconi R, Risica S (2013) A short review on radioactivity in drinking water as assessed by radiometric and Inductively coupled plasma-mass spectrometry techniques. Microchem J 107:95–100
6. Nguyen H, Jamali Moghadam M, Moayedi H (2019) Agricultural wastes preparation, management, and applications in civil engineering: a review. J Mater Cycles Waste Manag 21:1039–1051
7. Oluyinka OA, Oke EA, Oyelude EO et al (2022) Recapitulating potential environmental and industrial applications of biomass wastes. J Mater Cycles Waste Manag 24:2089–2107
8. Ashfaq A, Nadeem R, Bibi S, Rashid U, Hanif A, Jahan N, Ashfaq Z, Ahmed Z, Adil M, Naz M (2021) Efficient adsorption of lead ions from synthetic wastewater using agrowaste-based mixed biomass (potato peels and banana peels). Water 13(23):3344
9. Mokkapati RP, Ratnakaram VN, Mokkapati J (2019) Mass transfer, kinetic, equilibrium, and thermodynamic study on removal of divalent lead from aqueous solutions using agrowaste biomaterials, musa acuminata, casuarina equisetifolia L., and sorghum bicolor. Theoretic Found Chem Eng 53(4):578–590
10. Rwiza MJ, Oh S-Y, Kim K-W, Kim SD (2018) Comparative sorption isotherms and removal studies for Pb (II) by physical and thermochemical modification of low-cost agro-wastes from Tanzania. Chemosphere 195:135–145
11. Hasnaoui N, Wathelet B, Jiménez-Araujo A (2014) Valorization of pomegranate peel from 12 cultivars: dietary fibre composition, antioxidant capacity and functional properties. Food Chem 160:196–203
12. Abdel-Salam F, Yehia G, El-Zalaki E (2018) Characterization of wastes from pomegranate (Punica granatum L.) juice and its use as a functional drink. Egypt J Food Sci 46:91–100
13. Giri R, Kumari N, Behera M, Sharma A, Kumar S, Kumar N, Singh R (2021) Adsorption of hexavalent chromium from aqueous solution using pomegranate peel as low-cost biosorbent. Environ Sustain 4(2):1–17
14. Salam FA, Narayanan A (2019) Biosorption-a case study of hexavalent chromium removal with raw pomegranate peel. Desal Water Treat 156:278–291
15. Ruan J-H, Li J, Adili G, Sun G-Y, Abuduaini M, Abdulla R, Maiwulanjiang M, Aisa HA (2022) Phenolic compounds and bioactivities from pomegranate (Punica granatum L.) peels. J Agric Food Chem 70(12):3678–3686
16. Singh B, Singh JP, Kaur A, Singh N (2018) Phenolic compounds as beneficial phytochemicals in pomegranate (Punica granatum L.) peel: a review. Food Chem 261:75–86
17. Ververi M, Goula AM (2019) Pomegranate peel and orange juice by-product as new biosorbents of phenolic compounds from olive mill wastewaters. Chem Eng Proc-Proc Intensific 138:86–96
18. Reddy NA, Lakshmipathy R, Sarada N (2014) Application of Citrullus lanatus rind as biosorbent for removal of trivalent chromium from aqueous solution. Alex Eng J 53(4):969–975
19. Ben-Ali S, Jaouali I, Souissi-Najar S, Ouederni A (2017) Characterization and adsorption capacity of raw pomegranate peel biosorbent for copper removal. J Clean Prod 142:3809–3821
20. Ghaneian M, Bhatnagar A, Ehrampoush M, Amrollahi M, Jamshidi B, Dehvari M, Taghavi M (2017) Biosorption of hexavalent chromium from aqueous solution onto pomegranate seeds: kinetic modeling studies. Int J Environ Sci Technol 14(2):331–340
21. Mohammed T, Ibrahim R, Naji A (2018) Experimental investigation and thermodynamic study of heavy metal removal from industrial wastewater using pomegranate peel. In MATEC Web of Conferences. EDP Sci 162:05007
22. Chen Y, Wang H, Zhao W, Huang S (2018) Four different kinds of peels as adsorbents for the removal of Cd (II) from aqueous solution: Kinetics, isotherm and mechanism. J Taiwan Inst Chem Eng 88:146–151
23. Ömeroğlu Ay Ç, Özcan AS, Erdoğan Y, Özcan A (2012) Characterization of Punica granatum L. peels and quantitatively determination of its biosorption behavior towards lead(II) ions and Acid Blue 40. Colloids Surf B Bioint 100:197–220
24. Abbasi Z, Alikarami M, Homafar A (2009) Adsorption study on pomegranate peel: removal of Ni_{2+} from aqueous solution and Co_{2+}. Inorg Chem 3:3–6

25. Ay CO, Ozcan AS, Erdo˘gan Y, Ozcan A (2012) Characterization of Punica granatum L. peels and quantitatively determination of its biosorption behavior towards lead(II) ions and Acid Blue 40. Coll Surf B Bioint 100:197–204
26. Najim T, Yassin S (2009) Removal of Cr (VI) from aqueous solution using modified pomegranate peel: equilibrium and kinetic studies. J Chem 6:129–142
27. Jain N (2015) Removal of heavy metal by using different fruit peels, vegetable peels and organic waste—a review. Int J Adv Res 3(11):916–920
28. Bellahsen N, Varga G, Halyag N, Kertész S, Tombɔcz E, Hodur C (2021) Pomegranate peel as a new low-cost adsorbent for ammonium removal. Int J Environ Sci Technol 18:711–722
29. Guo L, Li G, Liu J, Meng Y, Xing G (2012) Nonlinear analysis of the kinetics and equilibrium for adsorptive removal of Cd(II) by starch phosphate. J Dispers Sci Technol 33:403–409
30. Lopez-Luna J, Ramirez-Montes LE, MartinezVargas S, Martinez AI, Mijangos-Ricardez OF, del Carmen A, González-Chávez M, Carrillo-González R, Solís-Domínguez FA, del Carmen Cuevas-Díaz M, Vázquez-Hipólito V (2019) Linear and nonlinear kinetic and isotherm adsorption models for arsenic removal by manganese ferrite nanoparticles. SN Appl Sci 1(950):1–19
31. Hashem A, Aniagor CO, Nasr MF, Abou-Okeil A (2021) Efficacy of treated sodium alginate and activated carbon fibre for Pb (II) adsorption. Int J Biol Macromol 176:201–216
32. Boukir A, Fellak S, Doumenq P (2019) Structural characterization of Argania spinosa Moroccan wooden artifacts during natural degradation progress using infrared spectroscopy (ATR-FTIR) and X-Ray diffraction (XRD). Heliyon 5(9):e02477
33. Mazlita Y, Lee H, Hamid S (2016) Preparation of cellulose nanocrystals bio-polymer from agro-industrial wastes: Separation and characterization. Polym Polym Compos 24(9):719–728
34. Li H, Qu Y, Xu J (2015) Microwave-assisted conversion of lignin. Production of biofuels and chemicals with microwave. Springer, pp 61–82
35. Hashem A, Hussein HA, Sanousy MA, Adam E, Saad EE (2011) Monomethylolated Thiourea—Sawdust as a new adsorbent for removal of Hg (II) from contaminated water: equilibrium kinetic and thermodynamic studies. Polym Plast Technol Eng 50(12):1220–1230
36. Hashem A, Fletcher AJ, El-Sakhawy M, Mohamed LA, Farag S (2020) Aminated hydroximoyl camelthorn residues as a novel adsorbent for extracting Hg(II) From contaminated water: studies of isotherm, kinetics, and mechanism. J Polym Environ 28(9):2498–2510
37. Aniagor C, Abdel-Halim E, Hashem A (2021) Evaluation of the aqueous Fe (II) ion sorption capacity of functionalized microcrystalline cellulose. J Environ Chem Eng 9(4):105703
38. Sokker E, Halim AS, Aly AH (2004) Cellulosic fabric wastes grafted with DMAEMA for the removal of direct dyes. Adsorpt Sci Technol 22(9):679–692
39. Aniagor CO, Afifi M, Hashem A (2021) Modelling of basic blue-9 dye sorption onto hydrolyzed polyacrylonitrile grafted starch composite. Carbohyd Polym Technol Appl 2:100141
40. Hashem A, Aniagor CO, Afifi MA-F, Abou-Okeil A, Samaha SH (2021) Synthesis of super-absorbent poly (AN)-g-starch composite hydrogel and its modelling for aqueous sorption of cadmium ions. Korean J Chem Eng 38(10):2157–2170